Three-Dimensional Solution Structure of Conotoxin ψ-PIIIE, an Acetylcholine Gated Ion Channel Antagonist[†,‡]

Scott S. Mitchell,[§] Ki Joon Shon,[||] Mark P. Foster,[§] Darrell R. Davis,[§] Baldomero M. Olivera,[⊥] and Chris M. Ireland*[,§]

Department of Medicinal Chemistry, University of Utah, Salt Lake City, Utah 84112, Department of Biology, University of Utah, Salt Lake City, Utah 84112, and Department of Physiology and Biophysics, Case Western Reserve University, 10900 Euclid Avenue, Cleveland, Ohio 44106

Received September 3, 1997; Revised Manuscript Received October 31, 1997

ABSTRACT: The three-dimensional structure of conotoxin ψ-PIIIE, a 24-amino acid peptide from *Conus purpurascens*, has been solved using two-dimensional (2D) ^{1}H NMR spectroscopy. Conotoxin ψ-PIIIE contains the same disulfide bonding pattern as the μ-conotoxins, which target skeletal muscle sodium channels, but has been shown to antagonize the acetylcholine gated cation channel through a noncompetitive mechanism. Structural information was obtained by the analysis of a series of 2D NOESY spectra as well as measurement of coupling constants from 1D ^{1}H and PE-COSY NMR experiments. Molecular modeling calculations included the use of the distance geometry (DG) algorithm, simulated annealing techniques, and the restrained molecular dynamics method. The resulting structures are considerably similar to the previously published structures for the μ-conotoxins GIIIA and GIIIB, despite the lack of sequence conservation between conotoxin ψ-PIIIE and the μ-conotoxins. The structure consists of a series of tight turns, each turn occurring in the position analogous to those of turns described in μ-GIIIA and μ-GIIIB. This suggests the disulfide bonding pattern is able to largely direct the structure of the peptides, creating a stable structural motif which allows extensive sequence substitution of non-cystine residues.

Conotoxin ψ-PIIIE is a recently described peptide toxin from the venom of the venomous snail *Conus purpurascens* that has been shown to act as a noncompetitive inhibitor of the acetylcholine receptor (*1*). ψ-PIIIE contains the same disulfide bonding pattern as the μ-conotoxins, though it shares no other sequence homology with this pharmacological class of peptides (Figure 1). Three-dimensional structures and analysis of structure−activity relationships have recently been published for the μ-conotoxins GIIIA (*2*−*4*) and GIIIB (*5*) describing a compact structure built around a cage of disulfide-bonded sulfur atoms. Replacement of individual non-cystine residues with alanine demonstrated voltage gated sodium channel binding activity for μ-GIIIA was particularly sensitive to mutations at residue R13 (*6*). This residue is not conserved between the sequences of μ-GIIIA and ψ-PIIIE, and the three-dimensional structure of ψ-PIIIE does not contain an equivalent functional group replacing the critical guanidinium group of R13 in μ-GIIIA. This result partially explains the altered binding specificity between the two peptides. The three-dimensional structure of conotoxin ψ-PIIIE is of particular interest, as differences in the structures will be useful in describing the structural requirements of the binding sites on the voltage gated sodium and the acetylcholine gated ion channels.

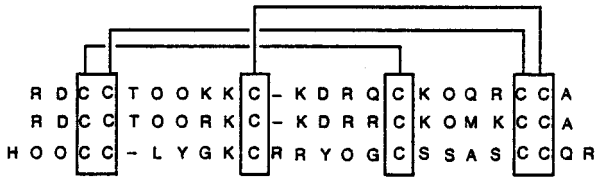

FIGURE 1: Aligned sequences of peptides μ-GIIIA, μ-GIIIB, and ψ-PIIIE showing disulfide bond connectivities. The C terminus of each peptide is amidated.

EXPERIMENTAL PROCEDURES

Sample. The peptide was synthesized using FMOC[1] solid phase peptide synthesis techniques. Cysteine residues were oxidized with glutathione as previously described (*7*). The resulting isomers were separated using reversed phase HPLC and tested for both biological activity and HPLC comigration with the native compound. The biological activity of the resulting material was found to be equivalent with that of the natural product.

NMR Spectroscopy. All spectra were recorded on a Varian Unity 500 MHz spectrometer equipped with a triple-channel waveform generator. The sample was prepared by dissolving 6 mg of the peptide in 475 μL of 90% H_2O/10% D_2O and

† Supported by NIH Grants P01 GM48677 and GM54710.

‡ Coordinates for the final structures have been deposited at the Brookhaven Protein Data Bank, Upton, NY 11973, under accession code 1as5.

§ Department of Medicinal Chemistry, University of Utah.

|| Case Western Reserve University.

⊥ Department of Biology, University of Utah.

[1] Abbreviations: 2D ^{1}H NMR, two-dimensional proton nuclear magnetic resonance spectroscopy; O, *trans*-4-hydroxyproline; NOESY, nuclear Overhauser effect spectroscopy; PE-COSY, primitive exclusive correlation spectroscopy; DQF-COSY, double-quantum filtered correlation spectroscopy; TOCSY, total correlation spectroscopy; DG, distance geometry; RMD, restrained molecular dynamics; RMA, relaxation matrix approach; IRMA, iterative relaxation matrix approach; T_1, longitudinal relaxation time; RMSD, root-mean-squared deviation; FMOC, fluorenylmethoxycarbonyl.

S0006-2960(97)02186-7 CCC: $15.00
Published on Web 02/03/1998

adjusting the pH to 3.5 using trifluoroacetic acid, or alternatively in 100% D_2O, to yield a 4.3 mM solution. All experiments were performed at 4.0 °C to decrease exchange rates of amide protons and lower the rotational correlation time (τ_c) of the peptide. NOESY (*8*), DQF-COSY (*9*), PE-COSY (*10*), and TOCSY (*11*) NMR spectra were collected in the phase sensitive mode using the hypercomplex method to achieve f_1 quadrature detection (*12*). Solvent suppression was achieved using presaturation by a 1.2 s Gaussian-shaped pulse centered on the H_2O signal during the relaxation delay. Data were collected using 4096 (t_2) × 512 (t_1) time domain data points for all experiments. NOESY experiments were performed using mixing times of 100, 200, and 400 ms in H_2O/D_2O (90%/10%) solutions, and with mixing times of 200 and 400 ms in 100% D_2O. ^1H T_1 values were measured using an inversion recovery experiment incorporating a presaturated water suppression pulse.

NOESY spectra were transformed with 4096 (f_2) × 2048 (f_1) frequency domain time points using the FELIX software package. The data were multiplied by a shifted sine bell squared function (60°), and the first data point in t_2 was linear predicted using the subsequent four data points. Cross-peak volumes were calculated by integration of all data points in a rectangular region which was manually defined for each peak. The NOE volumes were used directly in the IRMA calculations to derive distance constraints.

Structure Calculations. All structure calculations were performed using software included in the Insight II molecular modeling software package (Biosym Inc.) on a Silicon Graphics Indigo^2 workstation. A linear peptide structure was built using standard amino acid geometries, including disulfide bonds defined according to the experimentally determined pattern, which was used as a starting template to define the covalent structure of the peptide. Starting distance geometry structures were generated by metric-matrix embedding with random trial distances consistent with restraints from a smoothed bounds matrix as determined by the EMBED algorithm (*13*). Ten structures were generated in a given calculation, and resulting structures were superimposed on the structure with the lowest overall error function value.

The family of 10 structures generated by DG was then subjected to five rounds of IRMA (*14*, *15*) using 500 K MD for 10 ps, followed by 10 ps at 300 K and 100 and 1500 iterations of steepest and conjugate minimization, respectively. The RMA algorithm was then applied to the refined structures and the process repeated until *R*-factors no longer improved and no restraint violations greater than 0.5 Å were present in all 10 structures. The resulting constraint set was then used to generate a family of 50 DG structures which were then subjected to a simulated annealing protocol (*16*, *17*) described below.

The target function used for the restrained molecular dynamics (RMD) calculation is comprised of terms displayed in eq 1:

$$F_{\text{total}} = F_{\text{covalent}} + F_{\text{nonbond}} + F_{\text{NOE}} + F_{\text{chiral}} + F_{\text{dihedral}} \quad (1)$$

The final 50 distance geometry structures were initially subjected to 500 iterations of quartic and conjugate minimization, with all force constants reduced to 0.001 kcal mol^{-1} Å^{-2}. The RMD calculation is initiated with this weak force field, and NOE force constants are scaled up to 100% of their value and covalent force constants scaled to 15% of their values over 30 ps. The covalent and chiral terms were then increased to full value over an additional 10 ps of molecular dynamics. Finally, nonbond interactions and force constants for dihedral distance constraints were then scaled to 0.25 over 10 ps. The system was then cooled to 300 K according to a geometric progression over the final 10 ps of molecular dynamics. The resulting structures were then thoroughly minimized with all force constants at full value and the Lennard-Jones form of the nonbond force field using both steepest and conjugate minimization algorithms.

The family of 17 structures from the simulated annealing experiments which best satisfied the NOE data was then subjected to the RMA. The relaxation matrix predicted using the IRMA algorithm was viewed as a theoretical NOE spectrum and manually compared to experimental data for structures in a procedure known as back-calculation. Analysis of *R*-factor values computed over the ensemble of the 17 best structures also demonstrated the predicted RMA data agree well with experimental NOESY data.

RESULTS

Spectral Assignment. DQF-COSY and TOCSY NMR experiments were used to assign individual spin systems for each amino acid, which were then sequentially assigned by key NOESY cross-peaks in the fingerprint region using the method of Wütrich and co-workers (*18*). Application of these methods to the majority of the sequence was straightforward (Figure 2), except in the case of the three N-terminal amino acids. The amino-terminal protons of H1 were not observed, and amino acids O2 and O3 contain no amide protons. The residues were unambiguously assigned using the following NOE cross-peaks. The AMX H1 spin system was assigned on the basis of NOE cross-peaks from the aromatic H1 δ proton to the α and β protons, while the connectivity between H1 and O2 was determined by characteristic H1 α proton cross-peaks to the δ protons of O2, which is expected for a trans proline residue. The connectivity between O2 and O3 residues was demonstrated by NOE cross-peaks from the α to δ protons of O2 and O3, respectively. The α and amide protons of C4 show cross-peaks to the O3 δ protons, allowing the complete sequence assignment for all amino acids of the peptide.

Restraint Set Generation. Measurement of $^3J_{\text{NH}-\alpha}$ from the 1D ^1H spectrum were used to generate eight ϕ angle restraints, using the following criteria. Protons with coupling constants of less than 5 Hz (C4, C10, S17, and C21) were assigned angle restraints of −90° to −40°, and protons with coupling constants of greater than 8 Hz (C5, R11, and S18) were restrained to angles of −160° to −80°. No dihedral angle restraint violations were present in the set of 17 converged structures. Stereospecific β proton assignments were made by analyzing α to β coupling constants and NH to β and α to β NOE patterns to yield stereospecific assignments for C5, Y7, R12, Y13, C16, and Q23, and χ_1 angles were restrained to the range of −45° to −75° for these residues in accordance with the method of Hyberts et al. (*19*).

Initial molecular modeling calculations used distance constraints generated by categorizing NOE cross-peak volumes as strong, medium, or weak and assigning distance

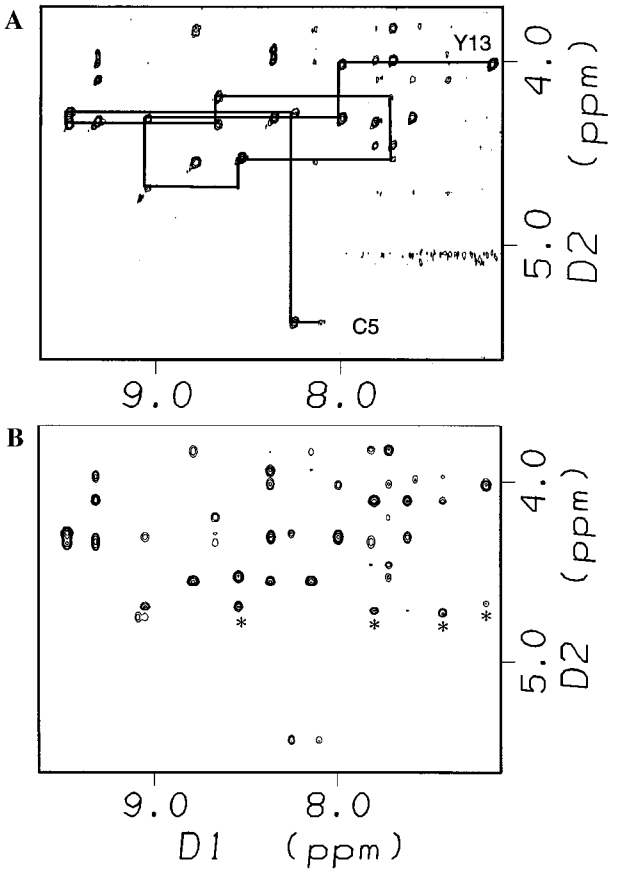

FIGURE 2: NH-α region of a 400 ms NOESY spectrum of conotoxin ψ-PIIIE. (A) The 400 ms NOE spectrum collected using presaturated water suppression with sequential connectivities shown for spin systems C5−Y13 (other connectivities are omitted for clarity). (B) The NH-α region of the back-calculated spectrum derived from the lowest-energy structure of conotoxin ψ-PIIIE. Cross-peaks marked with an * were observed in NOE spectra collected using gradient water suppression techniques.

constraints of 1.5−2.5, 2.5−3.5, and 3.5−5.5 Å based on these classifications. The structures generated using the resulting constraint set were not well converged, and showed significant restraint violations.

Subsequent molecular modeling calculations employed restraint sets generated using the IRMA process, described as follows. After assignment of cross-peaks in the NOESY spectrum, volume integrals were measured using the FELIX software package. These volumes were then used as input to the IRMA module of the Biosym molecular modeling software package. The τ_c was estimated by repeating the RMA calculation until the theoretical NOE buildup curve for β protons were in close agreement with the experimental buildup curves. The measured τ_c for the ω-conotoxin GVIA (*20*) was used as an initial starting point for this process, as the peptides are of similar size. The final values used were 0.6 ns for τ_c and 1.6 s for the T_1 leakage value. The IRMA algorithm individually calculates distance bounds for each assigned cross-peak, depending on the structural model. The distance restraints calculated by IRMA from the linear structure contain errors due to the poor approximation of the linear conformation to the final structure. To compensate for this, the lower-bound restraints were removed from this restraint set when applied to the initial distance geometry calculation. These distance constraints were used to generate

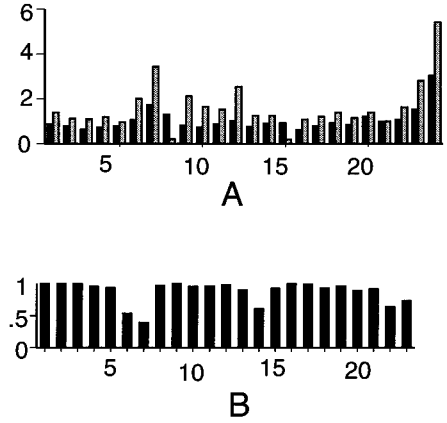

FIGURE 3: (A) RMSD values for backbone (shaded) and all (black) atoms of 17 converged structures computed against the mean structure. (B) The angular order parameter for ϕ angles of conotoxin ψ-PIIIE.

10 distance geometry structures, and this family of structures was then used to refine the distance constraints using the RMA algorithm. Five iterations of 500° MD and RMA were used to determine the final refined set of distance constraints which were used in the final calculation of 50 structures. The final set of restraints used in the simulated annealing calculation consisted of 269 distance constraints, 6 stereospecific assignments, and 10 ϕ angle constraints. The complete constraints set is provided in the Supporting Information. The overall degree of convergence generally corresponds with the distribution of distance constraints throughout the structure.

Structure Evaluation. The *R*-factor values calculated by the RMA process (*21*) give a quantitative assessment of the agreement between the experimental data and the resulting model. *R*-factors were observed to steadily decrease with refinement of the model, with ensemble *R*-factors of 0.98 for the initial linear peptide model to final values of 0.54 for the refined structure ensemble. Values for the parameter $R_{1/6}$ decreased from 0.11 for the linear structure to 0.008 for the final set of 17 structures.

RMSD values and the angular order parameter S_θ (*22*, *23*) were used to analyze the degree of convergence of the calculated structures. Figure 3 compares S_θ for ϕ angles and the RMSD values per residue for backbone atoms as well for the complete side chain. There are two main areas of conformational flexibility present in the structures, one centered about L6-Y7 as well as the two C-terminal residues. Neither L6 or Y7 shows long range NOEs to other portions of the molecule, so it is unclear whether the observed flexibility in the region arises from a paucity of NMR data or freedom of motion in solution. The decrease in the angular order parameter about residues O14 and G15 is not reflected in the RMSD values, as the conformational flexibility of the glycine residue does not displace side chain atoms to add to the overall RMSD for the residue.

Ramachandran plots may be used to judge the quality of a structure. Figure 4 displays a Ramachandran plot for the ϕ and ψ angles of the 17 best converged structures of conotoxin ψ-PIIIE. All of the dihedral angles fall in allowed regions according to the plot, demonstrating that both torsion angle and steric contact issues have successfully been resolved by the molecular modeling algorithms employed.

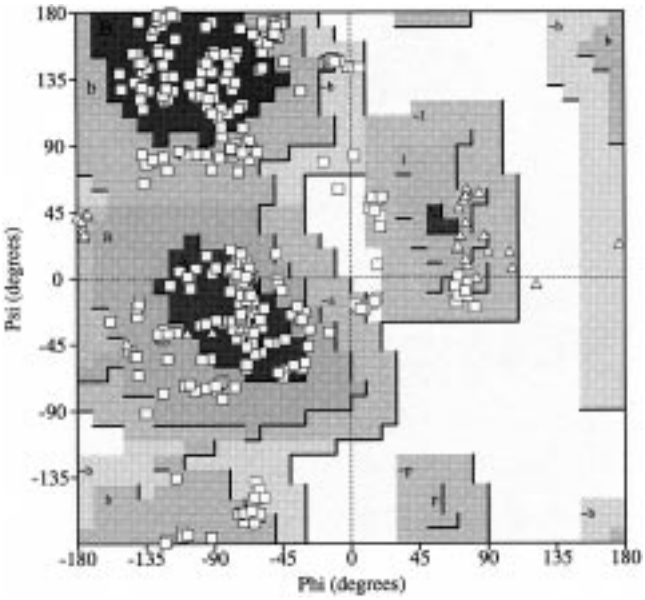

FIGURE 4: ϕ vs ψ Ramachandran plot including angles from the 17 converged structures of ψ-PIIIE. Squares signify non-glycine residues, and triangles signify glycine residues.

Description of the Structure. The structure of conotoxin ψ-PIIIE contains no α helix or β sheet regions, but consists of a series of β turns (Figure 5). A comparison of the positions of the β turns in μ-GIIIA and ψ-PIIIE reveals that each of the turns in conotoxin ψ-PIIIE occurs in the position analogous to that of the conserved cystine residues. Of particular interest, both pairs of adjacent cystine residues, C4-C5 and C21-C22, are the central residues of β turns; this structural feature is also observed in the two pairs of adjacent cystines in both the μ-GIIIA and μ-GIIIB structures. Other structural features include β turns between residues L6 and K9, Y13 and C16, C19 and A19, and A19 and C22. A γ turn appears between R11 and Y13, as well as a hydrogen bond between the carbonyl of C4 and the amide residue of R11.

^{1}H T_1 values, the dependence of the amide chemical shift on temperature, and amide exchange rates with D_2O were measured to assess the exchange rates for amide protons (Table 1). Analysis of these data for conotoxin ψ-PIIIE predicts seven protons are involved in hydrogen bonds, each of which can be explained by the secondary structure of conotoxin ψ-PIIIE. Amide protons of residues L6, K9, C16, A19, and C22 all appear to be hydrogen bonded to the carbonyl of the residue three amino acids earlier in the peptide sequence, with regular β turn geometries. The amide proton of Y13 is within hydrogen bonding distance of the carbonyl of R11, with residues R11, R12, and Y13 comprising a γ turn. The amide proton of R11 appears to be involved in a hydrogen bond with the carbonyl of C4 (Figure 6) in an interaction which may stabilize the chain reversal centered about residues L6 and Y7.

Table 1: Data Reflecting Exchange Rates of Amide Protons

NH	δ (ppm)	^{1}H T_1 (s)	$\Delta\delta/\Delta T$ (ppb/K)	slow exchange	turn
C4	9.05	1.02	7.3		
C5	8.08	1.05	6.4		
L6	8.23	0.98	6.1	*	O3−L6
Y7	9.45	0.84	9.1		
G8	8.65	0.69	6.5		
K9	7.70	1.04	4.0	*	L6−K9
C10	8.51	0.91	6.6		
R11	9.03	1.20	6.7	*	
R12	7.97	0.78	5.0		
Y13	7.16	1.21	3.8	*	R11−Y13
G15	8.77	0.85	5.1		
C16	8.12	1.07	2.4	*	Y13−C16
S17	8.35	0.82	6.7		
S18	7.70	1.03	3.3		
A19	7.80	1.04	3.1	*	C16−A19
S20	9.31	0.79	8.7		
C21	7.40	1.20	1.9		
C22	7.78	1.26	2.7	*	A19−C22
Q23	7.60	0.46	1.8		
R24	8.34	0.82	8.4		

Of the three disulfide bonds present in the sequence, only the side chains of C4 and C16 appear to be well resolved in the final 17 models of conotoxin ψ-PIIIE. This is consistent with the amount of spectral data available from NOESY and PE-COSY experiments for each of the cystine residues. Chemical shifts for β protons were observed to overlap for cystine residues C4, C5, and C10, complicating NOESY cross-peak assignments and coupling constant measurements. Cross-peaks across the disulfide linkage could be assigned

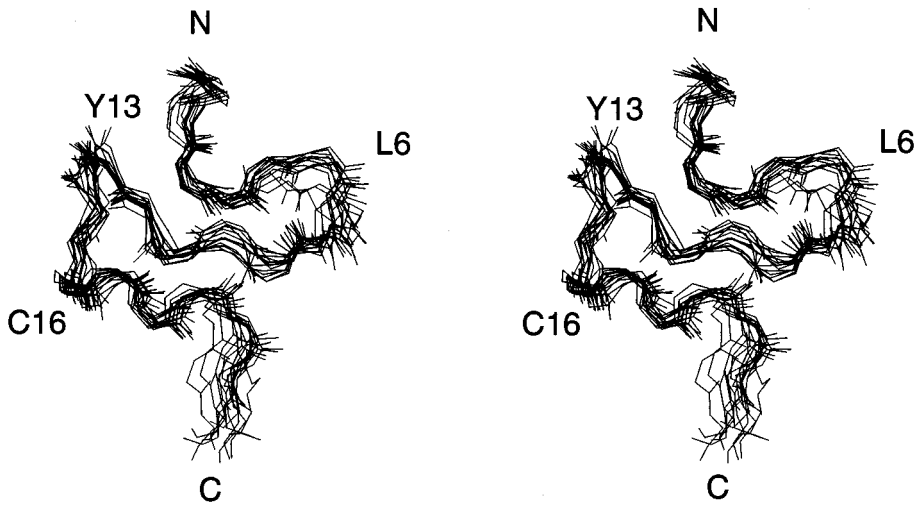

FIGURE 5: Stereoviews of the backbone atoms of the 17 converged structures of conotoxin ψ-PIIIE overlaid upon the lowest-energy structure after simulated annealing.

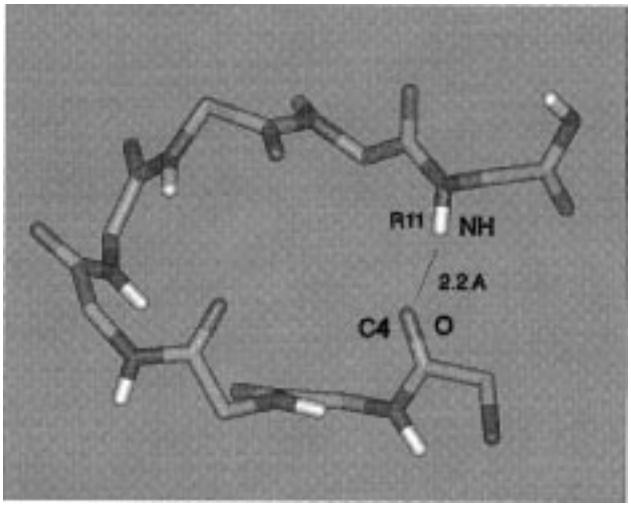

FIGURE 6: Backbone atoms of residues 4−11 showing the proposed hydrogen bond between the carbonyl and amide protons of C4 and R11, respectively.

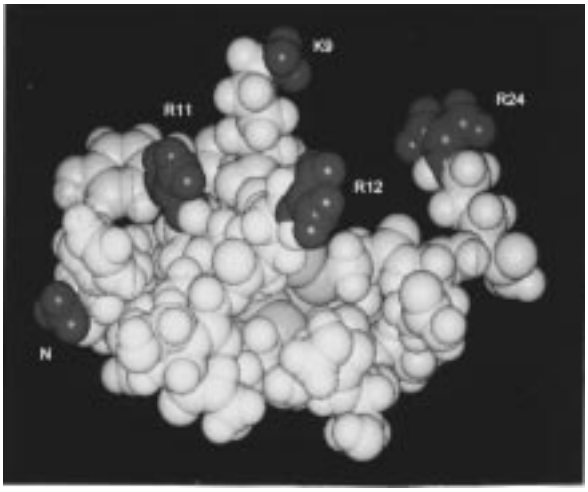

FIGURE 7: View of lowest-energy final structure displaying the five positively charged groups (blue atoms) of conotoxin ψ-PIIIE. At least one of the sulfur atoms (yellow) from each disulfide bond is visible.

only for C4−C16, and sufficient information for stereospecific β proton assignments was available for only C16. Regions of disorder throughout the model may be related to the lack of well-resolved spectral information to restrain key covalent disulfide linkages to specific conformations.

DISCUSSION

The positive charges are likely to be important for structure−activity relationships of conotoxin ψ-PIIIE, as the toxin targets the acetylcholine gated cationic channel. As with conotoxins μ-GIIIA and μ-GIIIB, ψ-PIIIE appears to have a flat, discoidal overall shape, with the majority of the positively charged residues congregated on one face of the molecule (Figure 7). It is reasonable to propose that the side of the structure containing the positively charged residues directly interacts with the toxin receptor. Side chain chemical shift values for K9, R12, and R24 are near the averaged values for residues which are fully exposed to solvent. The chemical shift of the guanidinium group of R11 is 6.69 ppm, which is shifted upfield from the equivalent groups of R12 and R24 by 0.4 ppm. The NMR structure of conotoxin ψ-PIIIE shows R11 is well defined throughout the side chain, and is less exposed to solvent than the other cationic groups of the peptide; this may be related to the hydrogen bond that appears between the amide proton of R11 and the carbonyl of C4.

A comparison of the structure of conotoxin ψ-PIIIE and NMR structures of μ-conotoxins μ-GIIIA and μ-GIIIB reveals considerable similarities in the three-dimensional structures of the peptides. Although μ-GIIIA and μ-GIIIB have extensive sequence homology, conotoxin ψ-PIIIE shares only the disulfide bonding pattern with the μ-conotoxins. This suggests that the disulfide bonding pattern alone may direct the secondary structural characteristics of the peptide, creating an amino acid backbone scaffold, upon which various amino acid side chains may be added without altering the overall structure of the peptide.

The differences in the receptor specificities for the μ-conotoxins and ψ-PIIIE demonstrate that *Conus geographus* and *C. purpurascens* have used the same structural backbone to target two different receptors. The importance of residue R13 in the binding activity of μ-GIIIA has been demonstrated (*6*), and a comparison of the primary sequences of ψ-PIIIE and μ-GIIIA confirms that this critical residue is not conserved between the two peptides. The three-dimensional structures of the two peptides demonstrate that, although the peptides have a similar overall shape, there is no equivalent functional group in ψ-PIIIE to play the role of R13 in μ-GIIIA. This explains why conotoxin ψ-PIIIE has no affinity for the voltage gated sodium channel, and future mutation studies should reveal the functional groups of conotoxin ψ-PIIIE that are necessary for activity at the acetylcholine gated ion channel.

Hill et al. (*24*) have suggested that the structures of μ-GIIIA and μ-GIIIB contain the core structural motifs of the cysteine-stabilized $\alpha\beta$ motif (CS$\alpha\beta$), which contains a helical region stabilized by disulfide bonds to cystine residues of a β strand (*24*). Although the secondary structures of μ-GIIIA, μ-GIIIB, and ψ-PIIIE are very similar, the secondary structure of ψ-PIIIE is best described as a series of turns, rather than in

FIGURE 8: Superimposed backbone diagrams for μ-GIIIA (*4*), μ-GIIIB (*5*), and ψ-PIIIE.

terms of α helices or β sheets. The μ-GIIIB structure described the 10 C-terminal amino acids as a distorted helix, on the basis of six slowly exchanging protons in this portion of the sequence. In conotoxin ψ-PIIIE, we observed three slowly exchanging amide protons in the analogous portion of the sequence, each of which is involved in three successive β turns. The similarity among the three-dimensional structures of conotoxins μ-GIIIA, μ-GIIIB, and ψ-PIIIE suggests that they define a stable and compact structural motif essentially independent of the CSαβ motif. Though the conserved disulfide bonding pattern is necessary for the structures of both the conotoxins and members of the CSαβ motif, the length of the non-cystine loops in the CSαβ motif are at least 10 amino acids longer in members of the CSαβ motif than in the conotoxins. This difference is reflected in the lack of well-defined secondary structure in each of the conotoxin structures. The conotoxin structures satisfy the structural constraints of the disulfide bonding pattern by employing a series of conserved β turns rather than the extensive α helical and β sheet structure present in members of the CSαβ motif. These structures may be useful for peptide engineering studies, as the similarity between the ψ-PIIIE structure and the μ-conotoxins demonstrates that the structure will tolerate extensive amino acid substitution in non-cystine residues.

These results suggest that structural features common to conotoxins μ-GIIIA, μ-GIIIB, and ψ-PIIIE define a structural motif unique to very small peptides, containing a cystine knot, which is stabilized by the presence of conserved β turns which create chain reversals necessary to satisfy the covalent restrictions of the cystine disulfide bonding pattern. Specifically, analysis of the secondary structure for the aligned sequences of the peptides shows that turns occur in the same position in each peptide relative to the cystine residues. The overall similarity in the backbone folding pattern of the three peptides is evident from comparison of the NMR stuctures shown in Figure 8. The similarity of μ-GIIIA, μ-GIIIB, and ψ-PIIIE, despite the lack of sequence conservation apart from the cystine knot, suggests that this is a stable structural motif has been used by *C. purpurascens* and *C. geographus* to target different biological receptors.

ACKNOWLEDGMENT

Partial funding for the Varian Unity 500 spectrometer was provided by NIH Grant S10RR06262. The operation of the NMR instrument is partially supported by an NCI Cancer Center grant.

SUPPORTING INFORMATION AVAILABLE

Complete ^{1}H NMR chemical shift assignments for PIIIE and an IRMA refined restraints set used for simulated annealing (10 pages). Ordering information is given on any current masthead page.

REFERENCES

1. Shon, K., Grilley, M., Jacobsen, R., Cartier, G. E., Hopkins, C., Gray, W. R., Watkins, M., Hillyard, D. R., Rivier, J., Torres, J., Yoshikami, D., and Olivera, B. M. (1997) *Biochemistry 36*, 9581.
2. Ott, K., Becker, S., Gordon, R. D., and Rüterjans, H. (1991) *FEBS Lett. 278*, 160.
3. Wakamatsu, K., Kohda, D., Hatanaka, H., Lancelin, J., Ishida, Y., Oya, M., Nakamura, H., Inagaki, F., and Sato, K. (1992) *Biochemistry 31*, 12577.
4. Lancelin, J., Kohda, D., Tate, S., Yanagawa, Y., Abe, T., Satake, M., and Inagaki, F. (1991) *Biochemistry 30*, 6908.
5. Hill, J. M., Alewood, P. F., and Craik, D. J. (1996) *Biochemistry 35*, 8824.
6. Sato, K., Ishida, Y., Wakamatsu, K., Kato, R., Honda, H., Ohizumi, Y., Nakamura, H., Ohya, M., Lancelin, J., Kohda, D., and Inagaki, F. (1991) *J. Biol. Chem. 266*, 26969.
7. Hopkins, C., Grilley, M., Miller, C., Shon, K., Cruz, L. J., Dykert, J., Rivier, J., Yoshikami, D., and Olivera, B. M. (1995) *J. Biol. Chem. 270*, 22361−22367.
8. Jeener, J., Meier, B. H., Bachman, P., and Ernst, R. R. (1979) *J. Chem. Phys. 71*, 4546−4553.
9. Rance, M., Sørensen, O. W., Bodenhausen, G., Wagner, G., Ernst, R. R., and Wütrich, K. (1983) *Biochem. Biophys. Res. Commun. 117*, 479−485.
10. Müller, L. (1987) *J. Magn. Reson. 72*, 191.
11. Braunschweiler, L., and Ernst, R. R. (1983) *J. Magn. Reson. 53*, 521.
12. States, D. J., Haberkorn, R. A., and Ruben, D (1982) *J. Magn. Reson. 48*, 286.
13. Crippen, G. M., and Havel, T. M. (1988) *Distance Geometry and Molecular Conformation*, Research Studies Press, Taunton, England.
14. Boelens, R., Koning, T. M. G., and Kaptein, R. (1988) *J. Mol. Struct. 173*, 299.
15. Boelens, R., Koning, T. M. G., van der Marel, G. A., van Boom, J. H., and Kaptein, R. (1989) *J. Magn. Reson. 82*, 290.
16. Clore, G. M., Nilges, M., Sukumaran, D. K., Brunger, A. T., Karplus, M., and Gronenborn, A. M. (1986) *EMBO J. 5*, 2729.
17. Nilges, M., Clore, G. M., and Gronenborn, A. M. (1988) *FEBS Lett. 239*, 129.
18. Wütrich, K. (1986) *NMR of Proteins and Nucleic Acids*, Wiley-Interscience, New York.
19. Hyberts, S. G., Marki, W., and Wagner, G. (1987) *Eur. J. Biochem. 164*, 625.
20. Davis, J. H., Bradley, E. K., Miljanich, G. P., Nadasdi, L., Ramachandran, J., and Basus, V. J. (1993) *Biochemistry 32*, 7396.
21. Gonzalez, C., Rullmann, J. A. C., Bonvin, A. M. J. J., Boelens, R., and Kaptein, R. (1991) *J. Magn. Reson. 91*, 659.
22. Hyberts, S. G., Golberg, M. S., Havel, T. S., and Wagner, G. (1992) *Protein Sci. 1*, 736.
23. Pallaghy, P. K., Duggan, B. M., Pennington, M. W., and Norton, R. S. (1993) *J. Mol. Biol. 234*, 405.
24. Cornet, B., Bonmatin, J., Hetru, C., Hoffmann, J. A., Ptak, M., and Vovelle, F. (1995) *Structure 3*, 435.

BI972186T